RSC Advances

PAPER

View Article Online
View Journal | View Issue

Cite this: *RSC Adv.*, 2022, **12**, 8617

The unique sandwich $K_6Be_2B_6H_6$ cluster with a real borozene B_6H_6 core†

Ying-Jin Wang, *[ab] Lin-Yan Feng,[ab] Miao Yan,[a] Chang-Qing Miao,[a] Su-Qin Feng[a] and Hua-Jin Zhai *[b]

Received 1st February 2022
Accepted 13th March 2022

DOI: 10.1039/d2ra00692h

rsc.li/rsc-advances

Theoretical evidence is reported for a boron-based $K_6Be_2B_6H_6$ sandwich cluster, showing a perfectly D_{6h} B_6H_6 ring, being capped by two tetrahedral K_3Be ligands. Due to the comfortable charge transfer, the sandwich is viable in $[K_3Be]^{3+}[B_6H_6]^{6-}[BeK_3]^{3+}$ ionic complex in nature. The $[B_6H_6]^{6-}$ core with 6π aromaticity vividly imitates the benzene (C_6H_6), occurring as a real borozene. In contrast, the tetrahedral $[K_3Be]^{3+}$ ligand is 2σ three-dimensional aromatic, acting as the simple superatom. Thus, this complex possesses a collectively three-fold 2σ/6π/2σ aromaticity. The interlaminar interaction is governed by the robust electrostatic attraction. The unique chemical bonding gives rise to interesting dynamic fluxionality.

1. Introduction

The electron-deficiency of boron leads to unconventional structures in its allotropes and compounds,[1–11] which is quite different from its neighbour carbon. The pure boron clusters favor the (quasi-)planar geometries over a wide range of sizes. Most of the planar boron clusters are controlled by the double (σ + π) aromaticity, especially, their π frameworks are analogous to those in benzene[1,12,13] or polycyclic aromatic hydrocarbons (PAHs).[14–17] The planar B_7^{3-}, B_8^{2-}, and B_9^- clusters[12,18–22] are representative, possessing the identical 6π aromaticity to $C_5H_5^-$, C_6H_6, and $C_7H_7^+$. Thus, they are endowed a relevant name of "borozene" by L. S. Wang, albeit that they are 6σ aromatic as well.[23] The "borozene" was first proposed for the planar $B_{12}H_6$ cluster by N. G. Szwacki.[24] Moreover, the metal-doped boron molecular wheels[25–30] and various inorganic benzene analogues[31,32] with double aromaticity are also widely investigated.

Strictly speaking, the real "borozene" is corresponding to the planar and aromatic $B_6H_6^{6-}$ ring, assuming as a derivative of C_6H_6 by replacing the C atom with B^-, just like the CH_4 and BH_4^- anion. However, the boron hydrides and their dianion species like forming the three-dimensional (3D) geometries, the latter are extremely stable with the 3D aromaticity.[33] Thus, it is more challenging to flatten the boron hydrides in chemistry. Additionally, the repulsion in highly charged $B_6H_6^{6-}$ is drastic, need to neutralize with the counter-cations. In 2003, A. I. Boldyrev computationally investigated the $Li_6B_6H_6$ cluster in the spirit of C_6H_6, providing a theoretical proof for existence of aromatic $B_6H_6^{6-}$ motif, albeit with a somewhat low D_{2h} symmetry.[34,35] The chemists have paid a lot of efforts into designing the transition metal centred M©B_6H_6 molecular wheels. Unfortunately, none of B_6H_6 motifs can be recognized as real "borozene" in view of the strong covalent interaction between the central metal atom and B_6H_6 ring, and abnormal charge distribution.[36–39] Last year, the author computationally reported a "Big Mac" sandwich of $Rb_6Be_2B_6$ cluster, consisting of a hexagonal B_6 ring and two tetrahedral Rb_3Be ligands, which skilfully mimics the style of ferrocene. The hexagonal B_6 core exists in the B_6^{6-} charge state with double 6π/6σ aromaticity, being sufficiently stable in the cationic field provided by two $[Rb_3Be]^{3+}$ ligands.[40] The bare planar B_6 ring as a structural motif has been found in the crystal structure of a solid state phase ($Ti_7Rh_4Ir_2B_8$),[41] and be discovered in some inverse sandwich clusters.[28,42,43] One interesting question arises, whether the planar $[B_6H_6]^{6-}$ ring can be stabilized in the similar field of counter-cation? If it is feasible, the real "borozene" will be achieved.

The target of present work lies in probing the viability of aromatic $[B_6H_6]^{6-}$ in $K_6Be_2B_6H_6$ cluster, which is consist of a perfectly planar B_6H_6 ring and two tetrahedral K_3Be ligands. The natural charge analyses show that $K_6Be_2B_6H_6$ cluster is a typical ionic complex, can be described by $[K_3Be]^{3+}[B_6H_6]^{6-}[BeK_3]^{3+}$ formula. The perfectly planar $[B_6H_6]^{6-}$ ring possesses the 6π aromaticity merely, occurring as a real "borozene". In contrast, the tetrahedral $[K_3Be]^{3+}$ ligand with 2σ delocalized electrons has the 3D aromaticity (or spherical aromaticity), serving as the superatom. Thus, this sandwich cluster has a collectively three-fold 2σ/6π/2σ aromaticity, whose three components are hold together *via* the robust electrostatic attraction. We believe that the stabilization of $[B_6H_6]^{6-}$

[a]*Department of Chemistry, Xinzhou Teachers University, Xinzhou 034000, Shanxi, China. E-mail: yingjinwang@sxu.edu.cn; hj.zhai@sxu.edu.cn*

[b]*Nanocluster Laboratory, Institute of Molecular Science, Shanxi University, Taiyuan 030006, China*

† Electronic supplementary information (ESI) available: Supplementary Table S1 and Fig. S1–S5, as well as a short movie for dynamic fluxionality extracted from the BOMD simulation. See DOI: 10.1039/d2ra00692h

borozene in $K_6Be_2B_6H_6$ complex is not an individual case. The planar aromatic $[B_5H_5]^{6-}$ and $[B_7H_7]^{6-}$ ring might be viable in such sandwich complexes.

2. Methods

We have theoretically designed a quaternary $K_6Be_2B_6H_6$ sandwich cluster basing on the concept of charge transfer and multifold aromaticity. The potential energy surface scan for $K_6Be_2B_6H_6$ cluster was performed using the Coalescence Kick (CK) algorithm[44,45] at the B3LYP/6-31G level, aiding with the manual constructions. Various possible initial structures were explored and fully reoptimized at the PBE0/6-311+G(d,p) level.[46] Vibrational frequencies were checked at the same level to guarantee that all presented isomers are true minima. The accurate energies of top five low-lying isomers at the PBE0/6-311+G(d,p) level were further estimated at the single-point CCSD(T)/6-311+G(d,p)//PBE0/6-311+G(d,p) level.[47] The transition state (TS) structures were searched using the QST2 method, and verified by intrinsic reaction coordinate (IRC) calculations.

For interpreting the stabilization of $K_6Be_2B_6H_6$ cluster, we have performed the Wiberg bond indices (WBIs) and natural atomic charges calculation using the NBO 6.0 program[48] at the PBE0/6-311+G(d,p) level. Chemical bonding was elucidated using the canonical molecular orbital (CMO), electron localization functions (ELFs),[49,50] and adaptive natural density partitioning (AdNDP) methods.[51] The AdNDP calculations were performed at the PBE0/6-31G level due to the low sensitivity to the theoretical level. The ELFs and AdNDP data were visualized using Molekel 5.4.0.8.[52] The nucleus-independent chemical shifts (NICSs)[53] were calculated at the PBE0/6-311+G(d,p) level. Born–Oppenheimer molecular dynamics (BOMD) simulations were performed at the PBE0/6-31G* level at the temperature of 300 and 600 K.[54] All electronic structure calculations and BOMD simulation were done using the Gaussian 09 package.[55]

3. Results and discussion

3.1. Geometric structures

Extensive structural searches and density functional theory calculations at the PBE0/6-311+G(d,p) level suggest that the $K_6Be_2B_6H_6$ cluster possesses two almost degenerated isomers (Fig. 1), the global minimum (GM) (D_{3d}, $^1A_{1g}$) and the closest low-lying isomer (LM) (D_{3h}, $^1A_1'$). Both isomers adopt the fascinating sandwich architectures, featuring a perfectly D_{6h} B_6H_6 ring being jammed by two tetrahedral K_3Be ligands. As a whole, two isomers are ingeniously assembled on the basis of the hierarchy of electronegativity. They are discrepant in assembling style of K_3Be ligands, a staggered fashion for GM and eclipsed one for LM. Their cartesian coordinates are given in Table S1 (ESI†). At the PBE0/6-311+G(d,p) level, D_{3d} ($^1A_{1g}$) GM is marginally more stable by 0.04 eV than D_{3h} ($^1A_1'$) LM with the zero-point energy (ZPE) corrections. Noted the dispersion corrections are not sensitive for present system according to the results at the PBE0-D3/6-311+G(d,p) level. The relative energies of two degenerated isomers were further refined at the CCSD(T)/6-311+G(d,p)//PBE0/6-311+G(d,p) level, which gives an energy distinction of 0.05 eV merely. The T_1 diagnostic factors of CCSD(T) for the GM and LM are 0.019, indicating the reliable CCSD(T) data. The other low-lying isomers (see Fig. S1, ESI†) are highly unstable, being at least 0.34 eV above the GM at the CCSD(T) level. Frankly, given the extremely complicated potential energy surface, we cannot completely ensure the true global minimum of the quaternary system. We have performed the minima hopping (MH)[56] search for this system (about 500 stationary points) as well, and did not find more stable isomers than the D_{3d} ($^1A_{1g}$) GM structure.

3.2. The bond distances, Wiberg bond indices and natural atomic charges

The bond distances for D_{3d} ($^1A_{1g}$) GM and D_{3h} ($^1A_1'$) LM at the PBE0 level are shown in Fig. 1. Two structures have almost identical bond distances, all of them are within 0.01 Å, apart from the K–K bonds (0.04 Å). Specifically, the B–B distances are 1.67 Å in the GM and 1.68/1.67 Å in the LM, respectively, being slightly shorter than the standard B–B single bond (1.70 Å).[57] The B–H bond distances are 1.23 Å. The B–Be/Be–K/K–K bond distances are distinctly longer than their referenced single bonds, suggesting the weak covalent interaction of them.

The WBIs for GM and LM structures are in accordance with the bond distances. The B–B bonds have the WBIs of 1.34 for the D_{3d} ($^1A_{1g}$) GM (Fig. S2(a), ESI†) and 1.35/1.33 for D_{3h} ($^1A_1'$) LM (Fig. S2(c), ESI†), being intermediate between the single and double bonds. Thus, they are dominated by the delocalized bonds apart from the two-center two-electron (2c–2e) σ bond. The WBIs of B–H bonds is 0.93, representing the normal single bond. The Be–K/K–K bonds with the nonnegligible WBIs of

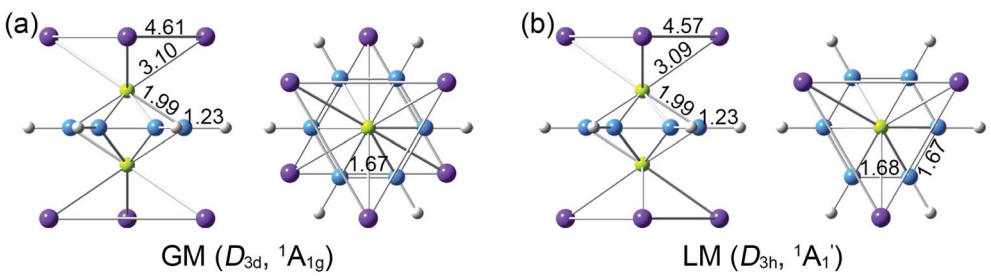

Fig. 1 Optimized geometries for (a) D_{3d} ($^1A_{1g}$) global-minimum (GM) and (b) D_{3h} ($^1A_1'$) low-lying isomer (LM) of $K_6Be_2B_6H_6$ cluster at the PBE0/6-311+G(d,p) level, along with the bond distances (in Å). Both side- and top-views are presented.

0.21/0.13 have somewhat strong covalent interaction than B–Be bonds, the WBIs of latter is negligible (only 0.07), which leads to an integrally tetrahedral K_3Be ligands in two isomers. Furthermore, the Be–K and K–K bonds in K_3Be ligand have a collective WBIs of 1.02, being in line with one four-center two-electron (4c–2e) bond.

As for the natural atomic charges, the D_{6h} B_6H_6 rings in D_{3d} ($^1A_{1g}$) GM and D_{3h} ($^1A_1'$) LM have the same charge distribution ($-0.91|e|$ for B and $-0.02|e|$ for H, see Fig. S2(b and d), ESI†). Thus, the B_6H_6 rings exist in the $[B_6H_6]^{6-}$ charged state, being isoelectronic with C_6H_6. The Be and K atom carries a positive charge of $+0.94|e|$ and $+0.63/0.62|e|$, respectively. The tetrahedral K_3Be ligand has a collectively positive charge of $+2.83/2.80|e|$, being in line with $[K_3Be]^{3+}$ species. Thus, both GM and LM could be viewed as the $[K_3Be]^{3+}[B_6H_6]^{6-}[BeK_3]^{3+}$ ionic complexes, in which the electron-deficiency of B_6H_6 is reasonably compensated by two tetrahedral K_3Be ligands.

3.3. Chemical bonding

In order to interpret the unique geometries and stability of the D_{3d} GM ($^1A_{1g}$) and D_{3h} ($^1A_1'$) LM sandwiches, we performed the systematic chemical bonding analyses for them. The D_{3d} GM ($^1A_{1g}$) has 34 valence electrons in total, occupying 17 CMOs (Fig. 2). According to their constituent atomic orbitals (AOs), these occupied CMOs are reasonably sorted into four subsets. In subset (a), there are six σ CMOs composed by the B 2s/2p AOs, which can be directly recombined as six Lewis 2c–2e B–B σ bonds. The six CMOs in subset (b) originated from the radical B 2p AOs and H 1s AOs are shown one-to-one correspondence with those in subset (a), which describes the six Lewis 2c–2e B–H σ bonds in nature. The subset (c) exhibits a perfectly π sextet on the D_{6h} B_6H_6 ring, faithfully mimicking that in organic benzene, although the degenerated HOMO−3/HOMO−3′ π CMOs have slight hybridization with the HOMO−2/HOMO−2′ σ CMOs in subset (b). Thus, the B_6H_6 ring possesses 6π aromaticity according to the $(4n + 2)$ Hückel rule. These 15 CMOs in subsets (a–c) with 30 occupying electrons are located on the B_6H_6 motif, supporting the assertation of $[B_6H_6]^{6-}$ charge state of NBO results. Two CMOs in subset (d) are clearly located on the two tetrahedral K_3Be ligands, which can be directly recombined into two 4c–2e σ bonds, one on each K_3Be tetrahedron. Thus, the tetrahedral K_3Be ligand has the 2σ 3D aromaticity according to $2(n+1)^2$ electron counting rule.[58] It can also be viewed as a superatom.[59,60]

On the whole, the CMOs in subsets (a) and (b) describe the interactions of B–B and B–H of B_6H_6 ring, being in line with its six localized B–B and B–H σ bonds. The CMOs in subsets (c) and (d) represent the delocalized frameworks, including of the 6π aromaticity on B_6H_6 ring and 2σ aromaticity on two K_3Be tetrahedrons, which collectively renders the three-fold (2σ/6π/2σ) aromaticity for the $[K_3Be]^{3+}[B_6H_6]^{6-}[BeK_3]^{3+}$ complex. The three-fold aromaticity underlies the stability of the GM structure. Moreover, the orbital component analysis suggests that HOMO-5 has a 14.2% Be 2s AOs contribution, in which two Be 2s AOs pretends to be the "p_z" style, taking part in the globally delocalized π bonding. As for the degenerated HOMO−3/HOMO−3′, there is a 12.0% Be $2p_x/2p_y$ AOs contribution, being bonding to the B $2p_z$ AOs of B_6H_6 ring. The minimal contribution of Be $2s/2p_x/2p_y$ AOs to three π CMOs is responsible for the extremely weak covalent interaction of B–Be bonds. The CMOs pattern of D_{3h} ($^1A_1'$) LM is similar to that in D_{3d} ($^1A_{1g}$) GM, and its degenerated π CMOs with less hybridization are more elegant (Fig. S3, ESI†).

The above CMOs bonding images of D_{3d} ($^1A_{1g}$) GM and D_{3h} ($^1A_1'$) LM are fully supported by the AdNDP analyses. As

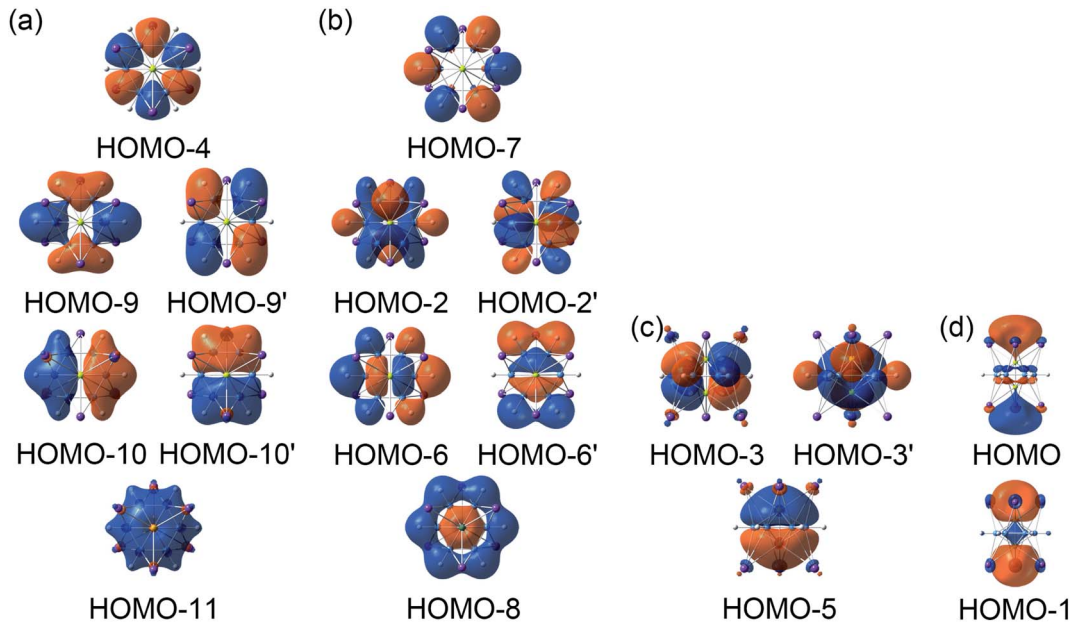

Fig. 2 Occupied canonical molecular orbitals (CMOs) of D_{3d} ($^1A_{1g}$) GM for $K_6Be_2B_6H_6$ cluster. (a) Six σ CMOs for six B–B σ bonds. (b) Six σ CMOs for six B–H σ bonds. (c) Three delocalized π CMOs on B_6H_6 ring. (d) Two σ CMOs over two tetrahedral K_3Be ligands.

shown in Fig. 3, the AdNDP result for the D_{3d} ($^1A_{1g}$) GM clearly reproduces six localized 2c–2e B–B and B–H σ bonds, as well as two delocalized 4c–2e σ bonds on tetrahedral K_3Be ligands and three delocalized six-center two-electron (6c–2e) π bonds on B_6H_6 ring. All the occupation numbers (ONs) are ideal. The delocalized σ and π frameworks further confirm the three-fold (2σ/6π/2σ) aromaticity of the system. Note that the scheme of 4c–2e σ bond in K_3Be tetrahedron is more rational than the alternative three-center two-electron (3c–2e) σ bond on K_3 triangle, the latter gives rise to a rather low ON of 1.48|*e*|. It means that Be atom has a remarkable 20.4% contribution to the 4c–2e σ bond, being close to K atom (26.5%).[40] The identical AdNDP bonding pattern is observed in the D_{3h} ($^1A_1'$) LM (Fig. S4†).

3.4. Interaction between B_6H_6 ring and tetrahedral K_3Be ligands

As mentioned above, the B_6H_6 ring and two tetrahedral K_3Be ligands are viable in hexavalent anion $[B_6H_6]^{6-}$ and trivalent cation $[K_3Be]^{3+}$, respectively. The interaction between the B_6H_6 ring and tetrahedral K_3Be ligands should be mainly dominated by the robust electrostatic attraction. We qualitatively estimate the ionic interaction by manually expanding the distances of two Be atoms to 10 Å, and subsequently performing a single-point calculation at the same level of theory. In this case, the energy difference with respect to the ground state structure is mainly attributed to the electrostatic attraction. The calculated ionic interaction energies are as high as 18.35 eV for the D_{3d} ($^1A_{1g}$) GM and D_{3h} ($^1A_1'$) LM. Thus, the sandwiches are quite stable against dissociation. Alternatively, we also estimated the electrostatic attraction between the $Be_2B_6H_6$ inverse sandwich and the two K_3 rings by separating the K_3 rings to 10 Å distance, which are 5.09 eV for the GM and 5.01 eV for LM, respectively.

Furthermore, we calculated the dissociation energy of $[K_3Be]^{3+}$ units in $K_6Be_2B_6H_6$ cluster according to the following formula, $[K_3Be]^{3+}[B_6H_6]^{6-}[BeK_3]^{3+}$ (D_{3d}, $^1A_{1g}$) = $[K_3Be]^{3+}[B_6H_6]^{6-}[BeK_2]^{2+}$ (C_s, $^1A'$) + K^+. The $[K_3Be]^{3+}[B_6H_6]^{6-}[BeK_2]^{2+}$ (C_s, $^1A'$) is obtained from the GM structure by removing a K atom, and performing a fully optimization using its anion state at the same level. Such calculation can be used to evaluate quantitatively the energetics of the combination of $[K_2Be]^{2+}$ and K^+ with respected to the tetrahedral $[K_3Be]^{3+}$ ligands in $K_6Be_2B_6H_6$ cluster. The result suggests that the dissociation energy of tetrahedral $[K_3Be]^{3+}$ is as high as 4.90 eV, hinting the tetrahedral $[K_3Be]^{3+}$ ligands is enough stable, and against disintegrating into the $[BeK_2]^{2+}$ and K^+ components.

3.5. The B_6H_6 ring in $K_6Be_2B_6H_6$ complex: a real borozene

The real "borozene" should accurately imitate the C_6H_6 in both molecular structure and chemical bonding. Bonding analyses indicate that the $K_6Be_2B_6H_6$ cluster can be described as $[K_3Be]^{3+}[B_6H_6]^{6-}[BeK_3]^{3+}$ complex. Here, the D_{6h} $[B_6H_6]^{6-}$ ring is isoelectronic with C_6H_6, possessing the identical π sextet and Lewis B–B/B–H σ bond skeletons with the C_6H_6 (Fig. 2(c) and 3). Actually, it is an example of electronic transmutation, the boron

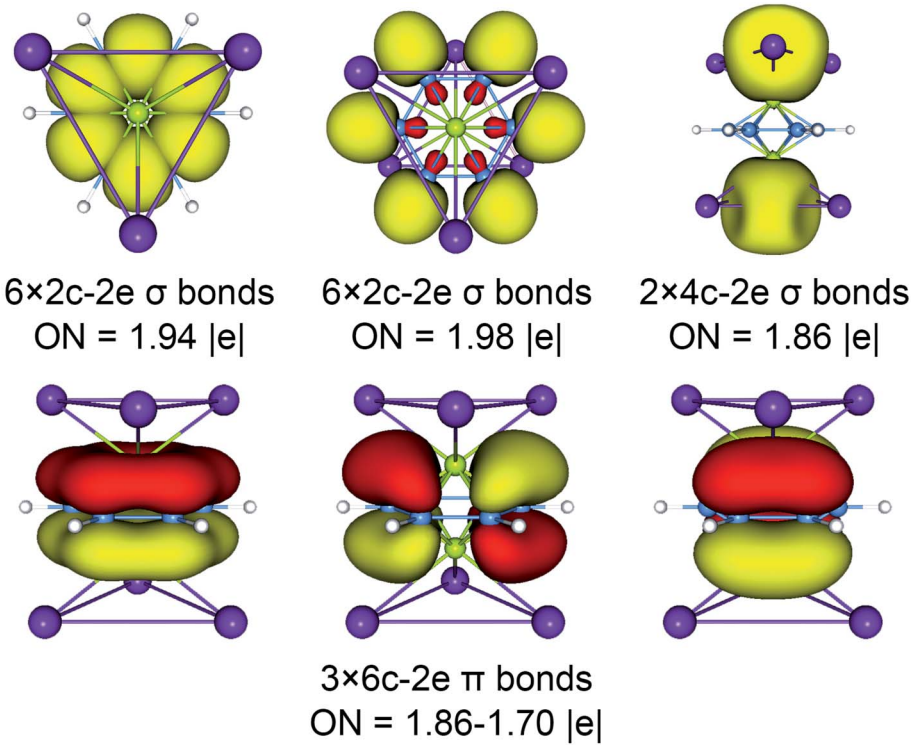

Fig. 3 Adaptive natural density partitioning (AdNDP) bonding pattern of D_{3d} ($^1A_{1g}$) GM for $K_6Be_2B_6H_6$ cluster. Occupation numbers (ONs) are indicated.

atom acquiring an extra electron is transmutated into the carbon.[61] Therefore, it truly occurs as a "borozene". The ELFs data provide the further theoretical proof. As shown in Fig. 4, the D_{6h} $[B_6H_6]^{6-}$ ring in the D_{3d} ($^1A_{1g}$) GM and D_{3h} ($^1A_1'$) LM exhibit the identical bonding patterns (ELF_σ and ELF_π) with the C_6H_6, despite the bifurcation value of ELF_π for the $[B_6H_6]^{6-}$ ring in D_{3d} ($^1A_{1g}$) GM is somewhat lower (0.58) (Fig. 4(a)), which is mainly attributed to the weak hybridization of π CMOs (as indicated above). Interestingly, the $[B_6H_6]^{6-}$ ring in D_{3h} ($^1A_1'$) LM presents an ideal bifurcation value (Fig. 4(b)), which positively confirms the 6π aromaticity of $[B_6H_6]^{6-}$ ring. Compared with the C_6H_6 (Fig. 4(c)), the D_{3d} ($^1A_{1g}$) GM and D_{3h} ($^1A_1'$) LM have two additional 4c–2e σ bonds on tetrahedral $[K_3Be]^{3+}$ ligands, being in line with their three-fold (2σ/6π/2σ) aromaticity, which are responsible for the stabilization for B_6H_6 and K_3Be components. The three-fold (2σ/6π/2σ) aromaticity in D_{3d} ($^1A_{1g}$) GM cluster is confirmed independently by the NICS calculation at the PBE0/6-311+G(d,p) level. The calculated NICS and $NICS_{zz}$ values are enough negative: −19.8 and −25.4 ppm for the center of K_3Be ligand, and −16.0 and −22.8 ppm for 0.5 Å above the center of B_6H_6 ring.

3.6. The dynamic fluxionality

The three-fold (2σ/6π/2σ) aromaticity and robust electrostatic attraction in the $[K_3Be]^{3+}[B_6H_6]^{6-}[BeK_3]^{3+}$ complex would facilitate interesting dynamic fluxionality of the cluster.[62–64] We obtained two TS structures (Fig. 5), D_{3d} ($^1A_{1g}$) TS_1 and D_{3h} ($^1A_1'$) TS_2, along with the displacement vectors for two soft vibrational modes of 46.2 and 24.7 cm^{-1} of the GM (Fig. S5(a)†). The TS_1 and TS_2 can be located from the GM by an independent rotation of 30° for B_6H_6 ring or an opposite rotation of 30° for each tetrahedral BeK_3 ligand with the B_6H_6 ring fixation, respectively. Alternatively, they also can be located from the LM by the similar operation. The LM structure has two soft vibrational modes of 58.8 and 8.9 cm^{-1} (Fig. S5(b)†), relating to the intramolecular rotations. At the PBE0/6-311+G(d,p) level, the TS_1 and TS_2 structures are 0.10 and 0.18 eV above the GM with the ZPE corrections, which are refined to 0.14 and 0.23 eV at the single point CCSD(T) level. The small energy barriers imply that the clusters are dynamically fluxional at room temperature. The structural evolution process is illustrated in Fig. 5. Two pathways are demonstrated for the rotation of B_6H_6 ring (blue line) and the

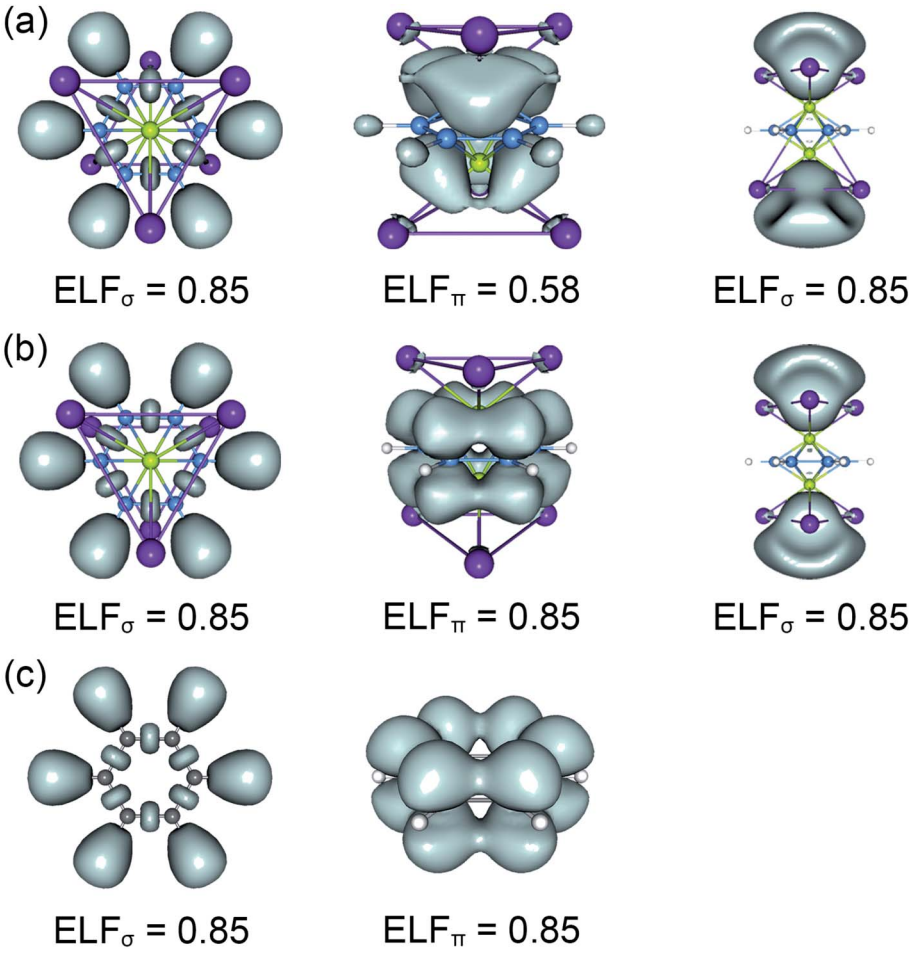

Fig. 4 Electron localization functions (ELFs) of (a) D_{3d} ($^1A_{1g}$) GM and (b) D_{3h} ($^1A_1'$) LM for $K_6Be_2B_6H_6$ cluster, and (c) D_{6h} ($^1A_{1g}$) C_6H_6. The images support the three-fold (2σ/6π/2σ) aromaticity of $K_6Be_2B_6H_6$ cluster and the assertion of borozene for B_6H_6 ring.

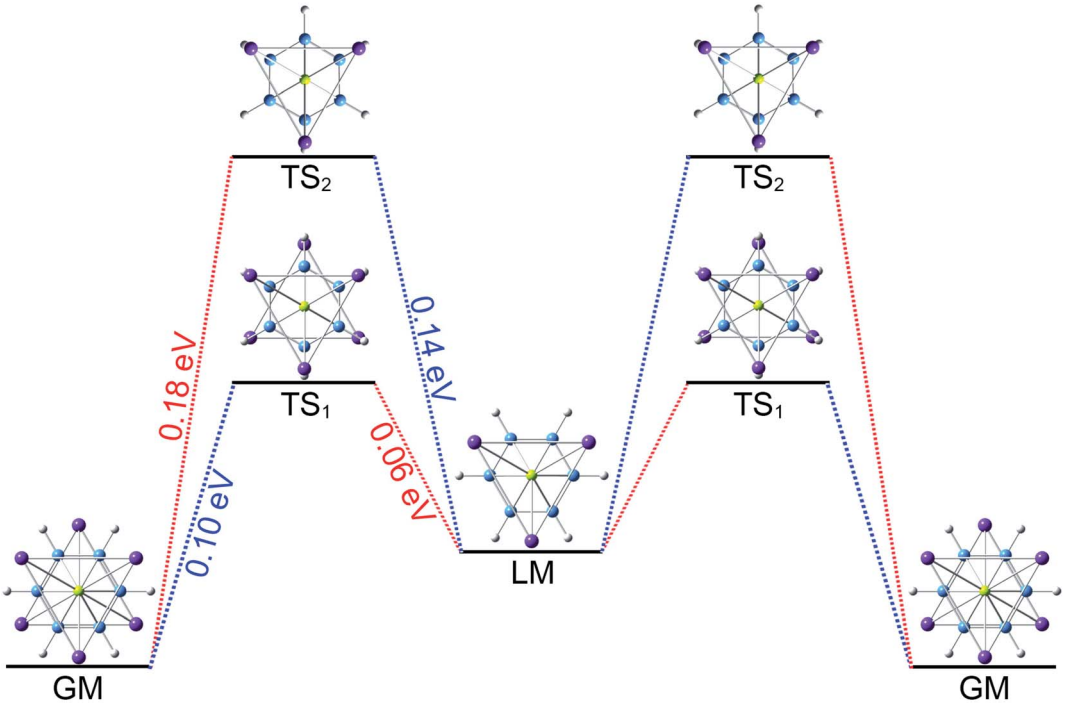

Fig. 5 Structural evolution of $K_6Be_2B_6H_6$ cluster during dynamic rotations. Two pathways are demonstrated for the rotation of B_6H_6 ring (blue curve) and the opposite rotation of two tetrahedral K_3Be ligands (red curve). The energy barriers of two transition state (TS) structures are 0.10 eV for TS_1 and 0.18 eV for TS_2 at the PBE0/6-311+G(d,p) level.

opposite rotation of two tetrahedral K_3Be ligands (red line). The BOMD simulation performed at the temperature of 300 K at the PBE0/6-31G* level faithfully confirm the above assessment (see the video in the ESI†), vividly demonstrating the fascinating dynamic structural fluxionality of the system. It should be noted that the structural integrity of $K_6Be_2B_6H_6$ cluster is maintained consistently even at the higher temperature of 600 K.

4. Conclusions

We have computationally designed a boron-based $K_6Be_2B_6H_6$ sandwich cluster, featuring a B_6H_6 ring being sandwiched by two tetrahedral K_3Be ligands. There is significant charge transfer from the K_3Be tetrahedrons to B_6H_6 ring (three electrons for each K_3Be), yielding the $[K_3Be]^{3+}[B_6H_6]^{6-}[BeK_3]^{3+}$ complex. The $[B_6H_6]^{6-}$ ring (with 6π delocalized electrons) precisely mimics the benzene in both geometry and chemical bonding, occurring as a real borozene. The tetrahedral $[K_3Be]^{3+}$ ligand with 2σ delocalized electrons possesses the three-dimensional aromaticity, serving as a superatom in essence. Overall, the sandwich cluster is a three-fold 2σ/6π/2σ aromatic system. The multi-fold aromaticity and robust electrostatic attraction among three motifs facilitates interesting dynamic fluxionality.

Conflicts of interest

There are no conflicts to declare.

Acknowledgements

This work was supported by the National Natural Science Foundation of China (21873058), the Natural Science Foundation of Shanxi Province (2018103), the Top Science and Technology Innovation Teams of Xinzhou Teachers University and the Fund for Shanxi "1331 Project" Key Subjects Construction.

References

1 H. J. Zhai, B. Kiran, J. Li and L. S. Wang, *Nat. Mater.*, 2003, **2**, 827–833.
2 S. Pan, J. Barroso, S. Jalife, T. Heine, K. R. Asmis and G. Merino, *Acc. Chem. Res.*, 2019, **52**, 2732–2744.
3 A. N. Alexandrova, A. I. Boldyrev, H. J. Zhai and L. S. Wang, *Coord. Chem. Rev.*, 2006, **250**, 2811–2866.
4 T. Jian, X. Chen, S. D. Li, A. I. Boldyrev, J. Li and L. S. Wang, *Chem. Soc. Rev.*, 2019, **48**, 3550–3591.
5 E. Oger, N. R. M. Crawford, R. Kelting, P. Weis, M. M. Kappes and R. Ahlrichs, *Angew. Chem., Int. Ed.*, 2007, **46**, 8503–8506.
6 W. Huang, A. P. Sergeeva, H. J. Zhai, B. B. Averkiev, L. S. Wang and A. I. Boldyrev, *Nat. Chem.*, 2010, **2**, 202–206.
7 H. J. Zhai, Y. F. Zhao, W. L. Li, Q. Chen, H. Bai, H. S. Hu, Z. A. Piazza, W. J. Tian, H. G. Lu, Y. B. Wu, Y. W. Mu, G. F. Wei, Z. P. Liu, J. Li, S. D. Li and L. S. Wang, *Nat. Chem.*, 2014, **6**, 727–731.
8 Y. J. Wang, Y. F. Zhao, W. L. Li, T. Jian, Q. Chen, X. R. You, T. Ou, X. Y. Zhao, H. J. Zhai, S. D. Li, J. Li and L. S. Wang, *J. Chem. Phys.*, 2016, **144**, 064307.

9 W. N. Lipscomb, *Science*, 1977, **196**, 1047–1055.
10 H. Braunschweig, R. D. Dewhurst and V. H. Gessner, *Chem. Soc. Rev.*, 2013, **42**, 3197–3208.
11 E. D. Jemmis, M. M. Balakrishnarajan and P. D. Pancharatna, *Chem. Rev.*, 2002, **102**, 93–144.
12 H. J. Zhai, A. N. Alexandrova, K. A. Birch, A. I. Boldyrev and L. S. Wang, *Angew. Chem., Int. Ed.*, 2003, **42**, 6004–6008.
13 Y. J. Wang, X. Y. Zhao, Q. Chen, H. J. Zhai and S. D. Li, *Nanoscale*, 2015, **7**, 16054–16060.
14 A. P. Sergeeva, D. Y. Zubarev, H. J. Zhai, A. I. Boldyrev and L. S. Wang, *J. Am. Chem. Soc.*, 2008, **130**, 7244–7246.
15 A. P. Sergeeva, Z. A. Piazza, C. Romanescu, W. L. Li, A. I. Boldyrev and L. S. Wang, *J. Am. Chem. Soc.*, 2012, **134**, 18065–18073.
16 Z. A. Piazza, H. S. Hu, W. L. Li, Y. F. Zhao, J. Li and L. S. Wang, *Nat. Commun.*, 2014, **5**, 3113.
17 Q. Chen, G. F. Wei, W. J. Tian, H. Bai, Z. P. Liu, H. J. Zhai and S. D. Li, *Phys. Chem. Chem. Phys.*, 2014, **16**, 18282–18287.
18 A. N. Alexandrova, H. J. Zhai, L. S. Wang and A. I. Boldyrev, *Inorg. Chem.*, 2004, **43**, 3552–3554.
19 T. R. Galeev, C. Romanescu, W. L. Li, L. S. Wang and A. I. Boldyrev, *J. Chem. Phys.*, 2011, **135**, 104301.
20 P. W. Fowler and B. R. Gray, *Inorg. Chem.*, 2007, **46**, 2892–2897.
21 L. L. Pan, J. Li and L. S. Wang, *J. Chem. Phys.*, 2008, **129**, 024302.
22 T. T. Chen, W. L. Li, T. Jian, X. Chen, J. Li and L. S. Wang, *Angew. Chem., Int. Ed.*, 2017, **56**, 6916–6920.
23 W. L. Li, T. T. Chen, W. J. Chen, J. Li and L. S. Wang, *Nat. Commun.*, 2021, **12**, 6467.
24 N. G. Szwacki, V. Weber and C. J. Tymczak, *Nanoscale Res. Lett.*, 2009, **4**, 1085–1089.
25 W. L. Li, C. Romanescu, T. R. Galeev, Z. A. Piazza, A. I. Boldyrev and L. S. Wang, *J. Am. Chem. Soc.*, 2012, **134**, 165–168.
26 W. L. Li, T. T. Chen, D. H. Xing, X. Chen, J. Li and L. S. Wang, *Proc. Natl. Acad. Sci. U. S. A.*, 2018, **115**, E6972−E6977.
27 W. L. Li, T. Jian, X. Chen, T. T. Chen, G. V. Lopez, J. Li and L. S. Wang, *Angew. Chem., Int. Ed.*, 2016, **55**, 7358–7363.
28 W. L. Li, L. Xie, T. Jian, C. Romanescu, X. Huang and L. S. Wang, *Angew. Chem., Int. Ed.*, 2014, **53**, 1288–1292.
29 Z. H. Cui, W. S. Yang, L. Zhao, Y. H. Ding and G. Frenking, *Angew. Chem., Int. Ed.*, 2016, **55**, 7841–7846.
30 C. Romanescu, T. R. Galeev, W. L. Li, A. I. Boldyrev and L. S. Wang, *Acc. Chem. Res.*, 2013, **46**, 350–358.
31 D. Z. Li, H. Bai, Q. Chen, H. Lu, H. J. Zhai and S. D. Li, *J. Chem. Phys.*, 2013, **138**, 244304.
32 L. Y. Feng, R. Li and H. J. Zhai, *Phys. Chem. Chem. Phys.*, 2019, **21**, 20523–20537.
33 J. Aihara, *J. Am. Chem. Soc.*, 1978, **100**, 3339–3342.
34 A. N. Alexandrova, K. A. Birch and A. I. Boldyrev, *J. Am. Chem. Soc.*, 2003, **125**, 10786–10787.
35 A. N. Alexandrova and A. I. Boldyrev, *Inorg. Chem.*, 2004, **43**, 3588–3592.
36 L. F. Li, C. Xu, B. K. Jin and L. J. Cheng, *J. Chem. Phys.*, 2013, **139**, 174310.
37 L. F. Li, C. Xu and L. J. Cheng, *Comput. Theor. Chem.*, 2013, **1021**, 144–148.
38 J. Hou, Q. Duan, J. Qin, X. Shen, J. Zhao, Q. Liang, D. Jiang and S. Gao, *Phys. Chem. Chem. Phys.*, 2015, **17**, 9644–9650.
39 H. L. Yu, R. L. Sang and Y. Y. Wu, *J. Phys. Chem. A*, 2009, **113**, 3382–3386.
40 Y. J. Wang, L. Y. Feng, L. Xu, X. R. Hou, N. Li, C. Q. Miao and H. J. Zhai, *Phys. Chem. Chem. Phys.*, 2020, **22**, 20043–20049.
41 B. P. T. Fokwa and M. Hermus, *Angew. Chem., Int. Ed.*, 2012, **51**, 1702–1705.
42 Y. J. Wang, C. Q. Miao, J. J. Xie, Y. R. Wei and G. M. Ren, *New J. Chem.*, 2019, **43**, 15979–15982.
43 Y. J. Wang, M. M. Guo, G. L. Wang, C. Q. Miao, N. Zhang and T. D. Xue, *Phys. Chem. Chem. Phys.*, 2020, **22**, 20362–20367.
44 M. Saunders, *J. Comput. Chem.*, 2004, **25**, 621–626.
45 P. P. Bera, K. W. Sattelmeyer, M. Saunders, H. F. Schaefer III and P. v. R. Schleyer, *J. Phys. Chem. A*, 2006, **110**, 4287–4290.
46 C. Adamo and V. Barone, *J. Chem. Phys.*, 1999, **110**, 6158–6170.
47 R. J. Bartlett and M. Musial, *Rev. Mod. Phys.*, 2007, **79**, 291–352.
48 E. D. Glendening, C. Landis and F. Weinhold, *NBO 6.0*, Theoretical Chemistry Institute, University of Wisconsin, Madison, 2013.
49 B. Silvi and A. Savin, *Nature*, 1994, **371**, 683–686.
50 T. Lu and F. Chen, *J. Comput. Chem.*, 2012, **33**, 580–592.
51 D. Y. Zubarev and A. I. Boldyrev, *Phys. Chem. Chem. Phys.*, 2008, **10**, 5207–5217.
52 U. Varetto, *Molekel 5.4.0.8*, Swiss National Supercomputing Center, Manno, Switzerland, 2009.
53 P. v. R. Schleyer, C. Maerker, A. Dransfeld, H. Jiao and N. J. R. v. E. Hommes, *J. Am. Chem. Soc.*, 1996, **118**, 6317–6318.
54 T. Helgaker, E. Uggerud and H. J. A. Jensen, *Chem. Phys. Lett.*, 1990, **173**, 145–150.
55 M. J. Frisch, *et al.*, *Gaussian 09, revision D.01*, Gaussian Inc., Wallingford, Connecticut, 2009.
56 S. Goedecker, *J. Chem. Phys.*, 2004, **120**, 9911–9917.
57 P. Pyykkö, *J. Phys. Chem. A*, 2015, **119**, 2326–2337.
58 M. Bühl and A. Hirsch, *Chem. Rev.*, 2001, **101**, 1153–1183.
59 A. C. Reber and S. N. Khanna, *Acc. Chem. Res.*, 2017, **50**, 255–263.
60 P. Jena and Q. Sun, *Chem. Rev.*, 2018, **118**, 5755–5870.
61 X. Zhang, K. A. Lundell, J. K. Olson, K. H. Bowen and A. I. Boldyrev, *Chem.–Eur. J.*, 2018, **24**, 9200–9210.
62 J. O. C. Jiménez-Halla, R. Islas, T. Heine and G. Merino, *Angew. Chem., Int. Ed.*, 2010, **49**, 5668–5671.
63 Y. J. Wang, J. C. Guo and H. J. Zhai, *Nanoscale*, 2017, **9**, 9310–9316.
64 J. C. Guo, L. Y. Feng, Y. J. Wang, S. Jalife, A. Vásquez-Espinal, J. L. Cabellos, S. Pan, G. Merino and H. J. Zhai, *Angew. Chem., Int. Ed.*, 2017, **56**, 10174–10177.